

# When Brain Foundation Model Meets Cauchy-Schwarz Divergence: A New Framework for Cross-Subject Motor Imagery Decoding

Jinzhou Wu, Baoping Tang, Qikang Li, Yi Wang, Cheng Li, Shujian Yu

**Abstract**—Decoding motor imagery (MI) electroencephalogram (EEG) signals, a key non-invasive brain-computer interface (BCI) paradigm for controlling external systems, has been significantly advanced by deep learning. However, MI-EEG decoding remains challenging due to substantial inter-subject variability and limited labeled target data, which necessitate costly calibration for new users. Many existing multi-source domain adaptation (MSDA) methods indiscriminately incorporate all available source domains, disregarding the large inter-subject differences in EEG signals, which leads to negative transfer and excessive computational costs. Moreover, while many approaches focus on feature distribution alignment, they often neglect the explicit dependence between features and decision-level outputs, limiting their ability to preserve discriminative structures. To address these gaps, we propose a novel MSDA framework that leverages a pretrained large Brain Foundation Model (BFM) for dynamic and informed source subject selection, ensuring only relevant sources contribute to adaptation. Furthermore, we employ Cauchy-Schwarz (CS) and Conditional CS (CCS) divergences to jointly perform feature-level and decision-level alignment, enhancing domain invariance while maintaining class discriminability. Extensive evaluations on two benchmark MI-EEG datasets demonstrate that our framework outperforms a broad range of state-of-the-art baselines. Additional experiments with a large source pool validate the scalability and efficiency of BFM-guided selection, which significantly reduces training time without sacrificing performance.

**Index Terms**—Motor imagery (MI), Brain-computer interface (BCI), Multi-source Domain Adaptation (MSDA), Brain Foundation Model (BFM), Cauchy-Schwarz Divergence.

## I. INTRODUCTION

**B**RAIN-COMPUTER interfaces (BCIs) establish a direct communication channel between the brain and external systems by interpreting neural activity without relying on neuromuscular pathways [1]. This technology offers transformative potential for patients with motor disabilities, including those resulting from spinal cord injuries [2], stroke-induced paralysis [3], or progressive neurodegenerative disorders [4]. Among various neural signals, electroencephalography (EEG) [5] has emerged as the predominant non-invasive BCI modality, due to its favorable trade-offs between safety, affordability, and millisecond-level temporal precision, making it suitable for clinical and everyday applications [6].

This work has been submitted to the IEEE for possible publication. Copyright may be transferred without notice, after which this version may no longer be accessible. (*Corresponding author: Baoping Tang.*)

Jinzhou Wu, Baoping Tang, Qikang Li, Yi Wang, and Cheng Li are with the State Key Laboratory of Mechanical Transmission, College of Mechanical and Vehicle Engineering, Chongqing University, Chongqing 400044, China (e-mail: paulwu@stu.cqu.edu.cn; bptang@cqu.edu.cn).

Shujian Yu is with the Department of Computer Science, Vrije Universiteit Amsterdam, 1081 HV Amsterdam, The Netherlands, and also with the Machine Learning Group, UiT–The Arctic University of Norway, 9019 Tromsø, Norway (e-mail: yusj9011@gmail.com).

Motor Imagery (MI) is the cognitive process of mentally simulating bodily movements without actual execution, during which the brain generates distinctive EEG patterns primarily within the  $\beta$  (18–26 Hz) and  $\mu$  (8–12 Hz) frequency bands localized over the motor cortex [7]. Decoding these MI-related EEG signals (MI-EEG) has become a cornerstone in non-invasive BCIs, especially for neurorehabilitation applications where real-time feedback during MI tasks supports motor recovery in patients with impairments such as stroke or spinal cord injury [8]. Traditional machine learning approaches for MI-EEG classification typically rely on manual feature extraction and extensive pre-processing steps [9], [10]. In contrast, deep learning techniques have demonstrated remarkable potential by automatically learning discriminative representations directly from raw EEG data, thereby improving classification accuracy and reducing the need for manual intervention [11]. Convolutional Neural Networks (CNNs) have been widely adopted for their ability to capture spatial-temporal EEG features [12], [13], while more recent Transformer-based architectures leverage self-attention mechanisms to model long-range dependencies and global contextual information in EEG signals [14]. Despite these advancements, MI-EEG decoding remains challenged by substantial inter-subject variability in brain activity patterns and the requirement for time-consuming, subject-specific calibration procedures, which hinder the practical deployment of BCIs [15].

To address the challenge of inter-subject variability and the limited availability of labeled data in MI-EEG decoding, domain adaptation (DA) techniques have been extensively investigated. DA aims to leverage knowledge from labeled source domains to improve learning in a target domain with scarce or no labels, which enables models trained on one or multiple subjects to generalize to unseen subjects [16]. Early DA methods primarily focus on aligning the marginal distributions of learned feature representations between source and target domains. This alignment is commonly achieved either explicitly through distance metric-based measures such as Maximum Mean Discrepancy (MMD) [17] or implicitly via adversarial training that employs domain discriminators to encourage indistinguishable feature distributions [18]. While these approaches reduce domain shifts at the feature level, they often overlook the dependence between features and their corresponding labels, which can lead to suboptimal performance. Therefore, subsequent efforts have sought to incorporate implicit alignment of conditional distributions or joint distributions to preserve class discriminability across domains [19], [20]. For example, Hong et al. [21] proposed a dynamic adversarial network (DJ DAN) and designed a local discriminator that aligns the conditional distribution from the

classifier predictions. Wei et al. [22] incorporated a transformer encoder and the spatiotemporal pattern differences to capture the global dependencies of EEG signals to improve discriminability and transferability of cross-subject MI decoding.

Recent studies suggest that leveraging diverse data from multiple source domains can improve model robustness and generalization, which has led to the development of multi-source domain adaptation (MSDA) approaches. For instance, Liu et al. [23] proposed a unified framework where each source and target subject is assigned a domain adversarial neural network (DANN), with the final prediction obtained by weighting the outputs of all source models. Such methods indiscriminately incorporate all available source domains, leading to scalability issues and escalating computational overhead as the number of sources grows. Additionally, inter-subject variability is pronounced in EEG signals, and irrelevant sources may introduce negative transfer effects. To mitigate this, some studies have explored source selection strategies. For example, Adaptive Source Joint Domain Adaptation (ASJDA) [24] filters source domains with Jensen-Shannon (JS) divergence computed on raw EEG data and employs Differential Entropy (DE) features as model inputs. Nevertheless, JS divergence on raw EEG signals can be unreliable in high-dimensional spaces, and DE relies on the assumption that EEG signals follow a Gaussian distribution, which may not hold in practice. These limitations highlight the need for an MSDA framework that can reliably assess source relevance and leverage theoretically grounded DA measures to achieve efficient, robust, and discriminative cross-subject EEG decoding.

In this work, we propose a novel MSDA framework that leverages a pretrained large Brain Foundation Model (BFM) to dynamically select the most relevant source subjects. The BFM's generalizable encoder, trained on diverse neural observations, provides a robust basis for quantifying inter-subject relevance in latent space. To further ensure precise alignment, we introduce Cauchy-Schwarz (CS) divergence and the conditional CS (CCS) divergence to simultaneously perform feature-level and decision-level alignment across domains. Unlike traditional metrics, CS/CCS divergences provide numerical stability and theoretical rigor for measuring both feature and output dependencies, explicitly mitigating domain shifts at both the representation and category levels. To our knowledge, this is the first work to integrate the representational power of large BFMs with CS divergence-based alignment in cross-subject MI-EEG decoding, offering a scalable and discriminative MSDA paradigm. The key contributions of this work are as follows:

- 1) We develop a source selection strategy that leverages generalizable BFM embeddings to identify relevant sources, reducing computational costs and negative transfer while maintaining performance.
- 2) We propose a joint-alignment MSDA method that simultaneously aligns feature spaces and decision boundaries using CS and CCS divergences, ensuring robust domain invariance and class discriminability.
- 3) Extensive experiments on two benchmark datasets demonstrate superior cross-subject decoding accuracy over state-of-the-art (SOTA) baselines. Moreover, the

scalability and practical value of our BFM-guided source selection strategy are validated in settings with a large source pool, which substantially reduces computational cost while maintaining strong performance, highlighting the critical role of informed source selection.

## II. RELATED WORKS

### A. EEG-based motor imagery classification

The advancement of machine learning has profoundly shaped the development of BCI systems. While conventional approaches demand laborious feature engineering and signal preprocessing [7], [10], deep learning paradigms have enabled end-to-end learning of discriminative features directly from raw EEG signals [25].

Innovations in CNNs have driven substantial progress in EEG decoding. Foundational works by [26] established deep ConvNet and Shallow ConvNet architectures with temporal-spatial filtering layers optimized for EEG's multidimensional characteristics. The subsequent EEGNet [27] introduced parameter-efficient depthwise convolutions while maintaining interpretability. Building on these principles, recent studies have enhanced model efficacy through multiple strategies: Borra et al. [28] developed Sinc-ShallowNet with spectrally-tuned convolutional kernels to improve both performance and interpretability; Chen et al. [11] addressed the location of critical EEG channels and designed an end-to-end channel selection strategy for MI recognition; Tao et al. [29] designed parallel CNN branches to extract multi-scale features and fuse them with self-attention module; Dang et al. [12] proposed an ensemble Flashlight-Net with dilated convolution to capture complementary information from  $\beta$  and  $\mu$  rhythms. These developments highlight an architectural evolution toward combining localized feature extraction with multi-level context modeling, significantly advancing MI classification performance.

Despite these advancements, the differences in brain anatomy, electrode placement, and mental states lead to significant domain shifts between the EEG data from different subjects. Traditional machine learning approaches often perform poorly when trained on data from one subject and tested on another, necessitating time-consuming calibration procedures for each new user [15]. This limitation has motivated the development of DA techniques specifically designed for cross-subject EEG classification.

### B. Domain Adaptation in Motor Imagery Classification

DA has become a powerful strategy to overcome the limitations of cross-subject EEG classification, enabling knowledge transfer from labeled source subjects to target subjects with no labeled data.

Early approaches to cross-subject EEG classification focused on projecting EEG data into a shared feature space to align marginal probability distributions. For example, Euclidean Alignment (EA) [30] has been proposed to directly align EEG trials from different subjects by transforming them into Euclidean space. Building on this concept, Liang and Ma [31] introduced a two-step calibration process working at both

subject and feature levels, where features from source and target subjects were fused by a dynamic adaptation algorithm in the Riemannian tangent space. To quantify and minimize domain discrepancies, MMD and other distance metrics have been widely adopted in DA. Zhang et al. [32] proposed a Manifold Embedded Knowledge Transfer (MEKT) approach that aligns EEG covariance matrices on a Riemannian manifold and performs DA by minimizing joint probability distribution shift via MMD while preserving geometric structures. Guo et al. [33] integrate a critic-free DA framework based on Nuclear-norm Wasserstein discrepancy (NWD) into a CNN framework to extract spatio-temporal features and align source-target domain distributions, thereby improving MI-EEG decoding.

Adversarial learning approaches have emerged as alternatives for DA in MI-EEG classification. To address the challenge of domain shift in raw EEG signals, Zhao [34] designed an end-to-end deep DA method with three jointly optimized modules, including a feature extractor, a classifier, and a domain discriminator, incorporating center loss to reduce intra-subject nonstationarity. Hong et al. [21] enhanced adversarial approaches by introducing DJDAN that balances marginal and conditional distribution alignment through adaptive weighting. Song et al. [35] employed the self-attention mechanism with adversarial learning to align the global dependencies of the EEG features between source and target subjects. While adversarial-based methods usually show competitive performance, they can be unstable during training and may require careful hyperparameter tuning.

There is a recent trend to leverage information from multiple source domains to improve target domain performance. Liu et al. [23] addressed the challenge of integrating multiple source domains by developing a unified multi-source optimization framework where the final classification result combines weighted predictions from multiple source domains. In MSDA, not all source subjects contribute equally to adaptation performance, and some may even lead to negative transfer. To address this issue, approaches such as Selective-MDA [36] and ASJDA [24] were proposed, which selectively limit the influence of source subjects based on their classification performance on the source domain and domain discrepancies with the target.

### C. Brain Foundation Model

The emergence of large Brain Foundation Models (BFMs) has revolutionized EEG analysis through large-scale self-supervised pretraining. Inspired by the success of large language models (LLMs), BFMs are pre-trained with a vast amount of physiological data to learn robust and generalizable neural representations, which have the potential to surpass traditional deep learning methods in understanding complex brain signals and generalizing across various tasks. Yi et al. [37] proposed a topology-agnostic framework that unifies varying EEG channel configurations through geometry-aware modeling, enabling effective cross-dataset pretraining. To enhance generalizability across BCI tasks, Jiang et al. presented LaBraM [38], a large-scale foundation model that segments EEG into channel patches and employs vector-quantized neural spectrum prediction for pretraining. Moreover, BrainWave

[39], which was trained in more than 40,000 hours of invasive and non-invasive brain recordings, was proposed to achieve SOTA performance in the diagnosis of neurological disorders. Most recently, Wang et al. proposed CBraMod [40], a criss-cross transformer that separately models spatial and temporal EEG dependencies, which leverages the comprehensive structural characteristics of EEG signals and can adapt to diverse EEG formats.

While these BFMs have demonstrated promising capabilities in learning universal EEG representations with preliminary applications in tasks such as disease diagnosis [39], speech intention decoding [41], and other neurophysiological tasks [38], their potential for DA in cross-subject MI decoding remains unexplored. Our study bridges this gap by proposing a novel framework that harnesses BFM-derived embeddings to quantify inter-subject similarity, thereby enabling effective source selection and distribution alignment for cross-subject DA.

## III. METHODOLOGY

This section presents the problem setup, notation, and the methodology of the proposed BFM-guided Multi-source Domain Adaptation (BFM-MSDA) framework for cross-subject motor imagery (MI) decoding tasks. Fig. 1 illustrates the overall framework and its key components.

### A. Problem Definition and Notations

Let  $\{D_s\}_{s=1}^S$  denote the labeled EEG datasets from a total of  $S$  source subjects, where the  $s$ -th subject's dataset is given by  $D_s = \{(\mathbf{x}_i^s, y_i^s)\}_{i=1}^{M_s}$ . Here,  $\mathbf{x}_i^s \in \mathbb{R}^{C \times T}$  represents an EEG trial with  $C$  channels and  $T$  time points, and  $y_i^s \in \{1, \dots, K\}$  is the class label corresponding to one of  $K$  MI tasks. The unlabeled EEG data from a target subject is denoted as  $D_t = \{(\mathbf{x}_j^t)\}_{j=1}^{M_t}$ .

The goal is to learn a model  $\mathcal{M} = g \circ f$ , where the feature extractor  $f: \mathbb{R}^{C \times T} \rightarrow \mathbb{R}^d$  maps raw MI-EEG signals to a latent representation with dimension  $d$ , and the classifier  $g: \mathbb{R}^d \rightarrow \{1, \dots, K\}$  outputs predicted class probabilities for MI tasks, such that  $\mathcal{M}$  generalizes effectively to  $D_t$  in an unsupervised DA setting.

### B. Preliminary Knowledge on Cauchy-Schwarz Divergence

Distributional alignment is critical for learning domain-invariant and discriminative representations in cross-subject MI-EEG decoding. However, this task remains challenging owing to the high dimensionality and continuous nature of the latent representations, as well as to the complex dependencies among EEG channels. Many previous DA methods focus on aligning class-conditional feature distributions  $p(\mathbf{x}|y)$  rather than posterior label distributions  $p(y|\mathbf{x})$ , due to relative simplicity of estimating  $p(\mathbf{x}|y)$  with  $y$  being a discrete variable. However, from a Bayesian standpoint, the joint distribution can be factorized as  $p(\mathbf{x}, y) = p(\mathbf{x})p(y|\mathbf{x})$ , indicating that aligning the joint distribution effectively requires separate alignment of both marginal feature distribution and conditional label distribution. Aligning  $p(\mathbf{x}|y)$  alone does not guarantee alignment of

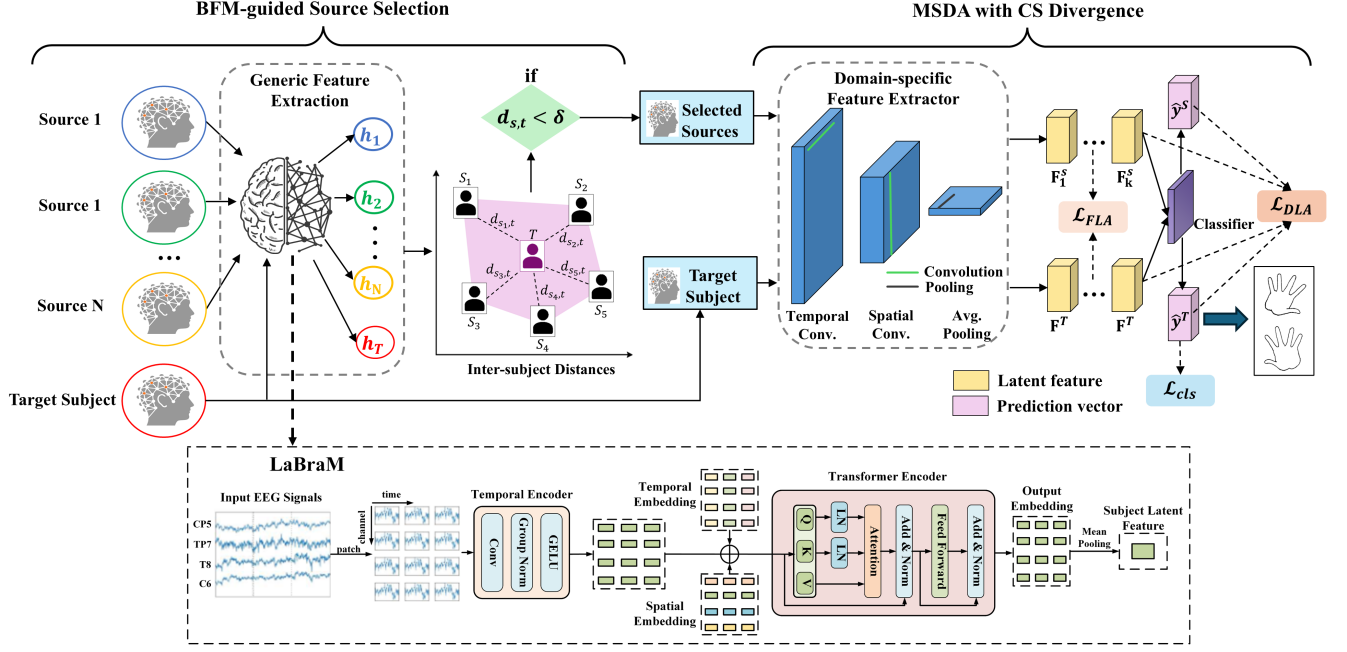


Fig. 1. Overview of the proposed BFM-MSDA framework for cross-subject motor imagery (MI) decoding. The framework comprises: (1) a source selection phase, where LaBraM, a representative brain foundation model, is employed to extract and hierarchically aggregate generic feature representations  $\mathbf{h}_1, \mathbf{h}_2, \dots, \mathbf{h}_S$  from  $S$  source subjects and  $\mathbf{h}_T$  from the target subject. Pairwise CS divergences  $d_{S_i, T}$  are computed between each source  $S_i$  and the target, and only sources with  $d_{S_i, T}$  smaller than a predefined threshold  $\delta$  are selected for adaptation; (2) a multi-source domain adaptation phase, in which feature-level alignment (FLA) is achieved by minimizing weighted CS divergences of the feature distributions  $p(z)$  between each selected source and the target, as well as between all pairs of selected sources. Decision-level alignment (DLA) is enforced by minimizing conditional CS divergences between the conditional label distributions  $p(y|z)$  of each source-target pair and all source-source pairs. (3) a trained classifier predicts MI class labels, such as left-hand and right-hand movement, for the target subject.

$p(y|x)$ , which directly relates to decision boundaries critical for MI decoding tasks.

The CS divergence derives from the Cauchy-Schwarz inequality for square-integrable functions  $p(x)$  and  $q(x)$ , which states:

$$\left[ \int p(x)q(x)dx \right]^2 \leq \int p^2(x)dx \int q^2(x)dx, \quad (1)$$

with equality holds only if  $p(x)$  and  $q(x)$  are linearly dependent. The CS divergence quantifies the discrepancy between  $p(x)$  and  $q(x)$  by taking the logarithm of the ratio between the squared inner product (left-hand side) and the product of their norms (right-hand side) of Eq. 2:

$$\begin{aligned} D_{CS}(p||q) &= -\log \left( \frac{|\int p(\mathbf{x})q(\mathbf{x})d\mathbf{x}|^2}{\int |p(\mathbf{x})|^2 d\mathbf{x} \int |q(\mathbf{x})|^2 d\mathbf{x}} \right) \\ &= -2 \log \left( \int p(\mathbf{x})q(\mathbf{x})d\mathbf{x} \right) + \log \left( \int p(\mathbf{x})^2 d\mathbf{x} \right) \\ &\quad + \log \left( \int q(\mathbf{x})^2 d\mathbf{x} \right). \end{aligned} \quad (2)$$

Obviously,  $D_{CS}(p||q) \geq 0$  with equality if  $p(x) = q(x)$ .

The CS divergence offers several advantages over other distance measures in DA: It is symmetric, has closed-form expressions for mixture-of-Gaussians (MoG) [42], and provides theoretically tighter generalization error bounds compared to Kullback-Leibler (KL) divergence [43]. CS divergence enables straightforward estimation without distributional

assumptions and demonstrates improved numerical stability compared to KL divergence (defined as  $D_{KL}(P \parallel Q) = \int p(x) \log \frac{p(x)}{q(x)} dx$ ), which diverges when  $q(x)$  approaches zero and  $q(x)$  is non-zero [44].

The conditional CS (CCS) divergence [45] extends the CS divergence to conditional distributions, which measures the discrepancy between two conditional distributions  $p(y|x)$  and  $q(y|x)$ , even though  $x$  is a high-dimensional continuous random variables, which makes it well suited for DA tasks:

$$\begin{aligned} D_{CCS}(p||q) &= -2 \log \left( \iint p(y|x)q(y|x) d\mathbf{x} dy \right) \\ &\quad + \log \left( \iint p^2(y|x) d\mathbf{x} dy \right) + \log \left( \iint q^2(y|x) d\mathbf{x} dy \right), \end{aligned} \quad (3)$$

In our scenario,  $x$  represents input EEG data or latent representations, and  $y$  denotes classification logits or probabilistic labels. Details on estimating CS and CCS divergences from a mini-batch of samples are provided in the Appendix.

### C. Source Selection with Brain Foundation Model

Negative transfer is a common issue in DA for MI decoding, often caused by substantial distributional differences across subjects. Indiscriminate use of all available source subjects during MSDA introduces negative transfer and excessive computational burden. To address this, our framework first selects source subjects whose EEG data distributions are similar to

that of the target subject with the guidance of BFM, thereby facilitating effective and positive knowledge transfer.

#### 1) Feature Extraction and Aggregation with LaBraM:

LaBraM [38] is a unified foundation model for EEG that facilitates cross-dataset learning through its unique approach of segmenting EEG signals into channel patches. Pretrained on roughly 2,500 hours of heterogeneous EEG data spanning 20 datasets, LaBraM acquires robust and generalizable neural representations. During pretraining, the model learns by reconstructing original neural codes from masked EEG channel patches, enhancing its ability to capture meaningful patterns in brain activity data. Importantly, the datasets used in our study were not included in the pretraining of LaBraM, ensuring that there is no risk of data leakage.

The process of extracting subject-level EEG representations using LaBraM is illustrated in the bottom panel of Fig. 1. Initially, each EEG recording is segmented into fixed-length, non-overlapping temporal patches, with each patch comprising 200 samples. For each patch, LaBraM extracts a latent feature vector that incorporates temporal and spatial embeddings, and processes these through transformer encoder layers with patch-wise attention to capture global dependencies. All patch vectors corresponding to each MI trial are then aggregated using mean pooling, resulting in a single trial-level feature vector. Subsequently, to obtain a stable subject-level representation, trial-level feature vectors from all sessions of the same subject are further averaged, yielding a unified 200-dimensional latent representation for each subject, suitable for subsequent discrepancy assessment.

2) *Source Selection via Inter-Subject Similarity:* For each source subject  $s$ , the aggregated subject-specific feature vector  $\mathbf{h}_s = \text{LaBraM}(D_s)$  is extracted, and similarly,  $\mathbf{h}_t = \text{LaBraM}(D_t)$  is obtained for the target subject, both using the pre-trained LaBraM-Base (5.8M parameters) model.

The distance between each source and the target subject is quantified by computing the CS divergence between their respective feature distributions:

$$d_{s,t} = D_{\text{CS}}(p(\mathbf{h}_s) \| p(\mathbf{h}_t)), \quad s = 1, \dots, S, \quad (4)$$

where  $S$  denotes the total number of candidate source subjects.

To ensure that only the most relevant sources are selected for each target, either a median-based or percentile-based threshold  $\delta$  can be applied to the set of computed distances  $\{d_{s,t}\}_{s=1}^S$ . The subset of source subjects  $\mathcal{S} \subseteq \{1, \dots, N\}$  is then defined as those with distances to the target below the threshold:

$$\mathcal{S} = \{s \mid d_{s,t} < \delta\}. \quad (5)$$

This approach excludes sources that are distant in feature space and retains only those that are most similar to the target.

#### D. Multi-source Domain Adaptation with CS Divergence

Let  $\mathbf{z} = f(\mathbf{x}) \in \mathbb{R}^d$  be the latent feature extracted by the feature extractor of the backbone network. We propose aligning both feature-level and decision-level distributions between source and target domains using CS divergence, which learns domain-invariant representations while ensuring consistent decision boundaries.

1) *Feature-level Alignment:* We first align the marginal distribution of learned features  $p(\mathbf{z})$ . Euclidean alignment (EA) [30] is applied to reduce inter-subject distribution discrepancy by aligning the EEG trials from each subject to a common reference space. EA is performed by calculating the arithmetic mean of covariance matrices  $R$  for the  $i$ th EEG trial of a subject:

$$\tilde{X}_i = \bar{R}^{-1/2} X_i, \quad (6)$$

where  $\bar{R} = \frac{1}{M} \sum_{i=1}^M X_i X_i^T$  and  $M$  represents the total number of EEG trials of the subject.

Different sources contribute unequally to adaptation. Therefore, we dynamically assign weights to the selected sources based on their CS divergence from the target:

$$\omega_s = \frac{\exp(-D_{\text{CS}}(p_s(\mathbf{z}) \| p_t(\mathbf{z})))}{\sum_{s'=1}^S \exp(-D_{\text{CS}}(p_{s'}(\mathbf{z}) \| p_t(\mathbf{z})))}, \quad \forall s \in \mathcal{S}. \quad (7)$$

where  $\mathcal{S}$  represents the subset of selected source domains.

The feature-level alignment (FLA) loss between source and target domains is then formulated as:

$$\mathcal{L}_{\text{FLA}}^{\text{ST}} = \sum_{s=1}^N \omega_s D_{\text{CS}}(p_s(\mathbf{z}) \| p_t(\mathbf{z})) \quad (8)$$

where  $\omega_s$  are the source weights obtained by Eq. (7) and  $N$  is the number of selected sources.

To reduce the heterogeneity among source domains, we also minimize the pairwise CS divergence between source domains:

$$\mathcal{L}_{\text{FLA}}^{\text{SS}} = \frac{2}{N(N-1)} \sum_{s=1}^N \sum_{s' > s}^N D_{\text{CS}}(p_s(y|\mathbf{z}) \| p_{s'}(y|\mathbf{z})), \quad (9)$$

Harmonizing the distributions across source subjects allows us to obtain a more unified source domain that facilitates better adaptation to the target. The overall FLA loss combines both components:

$$\mathcal{L}_{\text{FLA}} = \mathcal{L}_{\text{FLA}}^{\text{ST}} + \mathcal{L}_{\text{FLA}}^{\text{SS}}. \quad (10)$$

2) *Decision-level Alignment:* To ensure optimal discriminative performance on the target domain, we further align the decision boundaries using the CCS divergence. Similar to the FLA loss, the decision-level alignment (DLA) loss is calculated as:

$$\begin{aligned} \mathcal{L}_{\text{DLA}} = & \underbrace{\sum_{s=1}^N \omega_s D_{\text{CCS}}(p_s(y|\mathbf{z}) \| p_t(y|\mathbf{z}))}_{\mathcal{L}_{\text{DLA}}^{\text{ST}}} \\ & + \underbrace{\frac{2}{N(N-1)} \sum_{s=1}^N \sum_{s' > s}^N D_{\text{CCS}}(p_s(y|\mathbf{z}) \| p_{s'}(y|\mathbf{z}))}_{\mathcal{L}_{\text{DLA}}^{\text{SS}}}. \end{aligned} \quad (11)$$

where  $y$  denotes continuous classification logits produced by the backbone network.

### E. Classification and Overall Loss

Given one-hot labels  $\mathbf{y} = [y_1, y_2, \dots, y_K]$  for  $K$  MI tasks, the weighted classification loss on source data is computed as:

$$\mathcal{L}_{\text{cls}} = \sum_{s=1}^N \omega_s \sum_{i=1}^{M_s} \text{CE}(g(f(\mathbf{x}_i^s)), y_i^s), \quad (12)$$

where  $\{(\mathbf{x}_i^s, y_i^s)\}_{i=1}^{M_s}$  are the labeled samples from source subject  $s$ , and  $\text{CE}(\hat{\mathbf{y}}, \mathbf{y}) = -\sum_{c=1}^K y_c \log \hat{y}_c$  denotes the cross-entropy loss between predicted class probabilities  $\hat{\mathbf{y}} = g(f(\mathbf{x}))$  and one-hot label  $\mathbf{y}$ .

The total loss combines all components with dynamic weights  $\alpha_\tau$  and  $\beta_\tau$ :

$$\mathcal{L}_{\text{total}} = \mathcal{L}_{\text{cls}} + \alpha_\tau \mathcal{L}_{\text{FLA}} + \beta_\tau \mathcal{L}_{\text{DLA}}, \quad (13)$$

where

$$\alpha_\tau = \frac{\alpha \exp(-\tau + 100)}{1 + \exp(-\tau + 100)}, \quad \beta_\tau = \frac{\beta}{1 + \exp(-\tau + 100)},$$

with  $\alpha$  and  $\beta$  as hyperparameters balancing the losses, and  $\tau$  the current epoch. This scheme prioritizes the alignment of the FLA initially and gradually increases the contribution of the DLA. The pseudo-code of the proposed BFM-MSDA framework is given in Algorithm 1.

---

#### Algorithm 1 BFM-guided Multi-source Domain Adaptation (BFM-MSDA) Framework

---

**Input:** Labeled source EEG datasets  $\{D_s^i\}_{i=1}^S$ , unlabeled target EEG dataset  $D_t$ , pretrained LaBraM model, hyperparameters  $\alpha, \beta$ , training epochs  $E$

**Output:** Predicted class labels  $\hat{Y}_t$  for target data  $D_t$

- 1: **Stage 1: Source Selection with LaBraM**
  - 2: **for** each source subject  $i = 1$  to  $S$  **do**
  - 3:   Extract source feature vector:  $\mathbf{h}_i \leftarrow \text{LaBraM}(D_s^i)$
  - 4: **end for**
  - 5: Extract target feature vector:  $\mathbf{h}_t \leftarrow \text{LaBraM}(D_t)$
  - 6: **for** each source subject  $i = 1$  to  $S$  **do**
  - 7:   Compute pairwise distances  $d_{s,t}$  by Eq. (4)
  - 8: **end for**
  - 9: Select subset of sources  $\mathcal{S} \subseteq \{1, \dots, N\}$  with  $d_{s,t}$  below percentile threshold
  - 10: Initialize model parameters for  $f$  and  $g$
  - 11: **Stage 2: Multi-source Domain Adaptation**
  - 12: **for** epoch  $\tau = 1$  to  $E$  **do**
  - 13:   Compute source weights  $\omega_s$  for  $s \in \mathcal{S}$  by Eq. (7)
  - 14:   Compute  $\mathcal{L}_{\text{FLA}}$  by Eq. (10)
  - 15:   Compute  $\mathcal{L}_{\text{DLA}}$  by Eq. (11)
  - 16:   Compute classification loss  $\mathcal{L}_{\text{cls}}$  by Eq. (12)
  - 17:   Update model parameters by minimizing Eq. (13)
  - 18: **end for**
  - 19: **return** classification results  $\hat{Y}_t = g(f(D_t))$  for target
- 

## IV. EXPERIMENTS

### A. Datasets and Preprocessing

The effectiveness of the proposed framework is assessed using two public EEG datasets collected under different conditions, with distinct devices, subject groups, and sample sizes.

1) *Dataset I: BCI Competition IV 2a Dataset:* The BCI Competition IV 2a dataset [46] comprises EEG recordings from nine subjects performing four-class MI tasks involving left hand, right hand, feet, and tongue movements. Data were acquired using 22 Ag/AgCl electrodes positioned according to the standard 10-20 system. Originally sampled at 250 Hz, the signals were subsequently downsampled to 200 Hz and filtered with a 0.5–40 Hz bandpass. For our analysis, we exclusively used left- and right-hand MI trials from each subject's first session (144 trials per subject), focusing on the 3–6 second post-stimulus window.

2) *Dataset II: GigaDB Dataset Subset:* The GigaDB EEG dataset [47] includes recordings from 52 healthy subjects (s1-s52), each performing right-hand and left-hand MI with 100 trials per class. Each MI trial lasted 3 seconds. EEG signals were recorded from 64 channels at 512 Hz and subsequently downsampled to 200 Hz and band-pass filtered between 0.5 and 40 Hz. Given the large number of subjects and considerable variability in individual transferability, a representative and compact subset of 10 subjects was selected by a greedy selection algorithm. Firstly, inter-subject distances were computed using CS divergence. Then, starting from the subject with the smallest average distance to all others, we iteratively added the subject that minimized the increase in the total pairwise distance within the subset. The resulting subset included s3, s5, s15, s18, s29, s31, s41, s43, s45, and s46, which had the smallest total intra-subset distance among all possible combinations. This subset constitutes Dataset II for our experiments.

### B. Baseline Methods

The proposed framework is compared against a variety of classic and SOTA methods, including: 1) **EEG-specific baseline models:** EEGNet [27] and ShallowConvNet [26]; 2) **Unsupervised DA techniques:** JAN [18], DJP-MMD [20], and DJDAN [21]. The backbone is the same as the EEGNet baseline model; and 3) **MSDA methods:** GAT [35] and ASJDA [24], with EEGNet as the backbone model.

### C. Experimental Protocol and Setup

1) *Cross-subject leave-one-subject-out (LOSO) validation:* To simulate the cross-subject adaptation scenario, we follow a LOSO evaluation protocol. For Datasets I and II, each subject is sequentially designated as the unlabeled target domain, while the remaining subjects in the dataset serve as potential source domains. Instead of utilizing all available source subjects, the proposed source selection method first identifies relevant source subjects with high similarity to the target. A 50th percentile threshold is used to filter relevant sources. This process is repeated for all subjects to ensure robustness and generalization of the proposed framework.

2) *Selective MSDA under large source base:* To further validate the effectiveness and practicality of the proposed source selection strategy, an additional experiment simulates a real-world scenario in which a large database of source subjects is available. In this experiment, the 10 subjects from Dataset II are treated as target domains, while the remaining 42

subjects from the expansive GigaDB dataset serve as potential source domains. Our source selection approach is applied with a more stringent threshold set at the 25th percentile, resulting in approximately 10 to 13 selected source subjects for each target. DA is then conducted exclusively using these selected sources. For comparison, we conduct parallel experiments using randomly selected groups of 12 source subjects (5 different random groups in total) to benchmark the benefit of informed source selection. All other experimental conditions remain consistent with the LOSO validation setup. For this experiment, the Wilcoxon signed-rank test is conducted to analyze the statistical significance of performance comparisons.

EEGNet is used as the backbone network for DA experiments, with its temporal kernel size set at 100, corresponding to half the EEG sampling rate [27]. The balancing factors for the losses are fixed at  $\alpha = 0.7$  and  $\beta = 1.4$  for both datasets. For optimization, we employ the Adam optimizer with a learning rate of 0.001 and a batch size of 32 for both datasets. To enhance training stability and convergence, we incorporate the Cosine Annealing learning rate scheduler. The number of training epochs is set at 500 for Dataset I and 300 for Dataset II. The kernel sizes  $\sigma$  of the Gaussian kernels for the CS divergence and MMD-based methods are determined in a multi-kernel manner proportional to the pairwise distances between samples. All experiments are implemented using PyTorch in Python and executed on an NVIDIA RTX 4070Ti GPU.

The classification accuracy and Cohen’s kappa value are used to evaluate the classification performance of the student models. Kappa is defined as follows:

$$\kappa = \frac{p_o - p_e}{1 - p_e} \quad (14)$$

where  $p_o$  represents the observed accuracy and  $p_e$  denotes the accuracy by chance. All methods are trained and evaluated in 10 repeated runs with random initialization.

## V. RESULTS

### A. Cross-subject Classification Performances

The cross-subject classification accuracies and kappa values on Dataset I and Dataset II are summarized in Tables I and II, respectively. The proposed framework consistently outperforms all baseline methods in terms of average performance on both datasets, demonstrating its superior generalization capability across subjects with varying EEG patterns. On Datasets I and II, our method achieves the best performance on most target subjects. The improvement is particularly notable for subjects who originally exhibit lower decoding performance on the baseline model, indicating the framework’s robustness in handling challenging cases.

The integration of the pretrained BFM (LaBraM) for source selection ensures that only the most relevant source subjects contribute to adaptation, effectively mitigating negative transfer. Furthermore, the use of CS divergence for multi-source alignment allows precise matching of both marginal feature distributions and conditional decision boundaries, resulting in a more discriminative and domain-invariant representation.

Compared to classical MI decoding models such as EEGNet and ShallowConvNet, which do not explicitly address domain shifts, our method’s DA strategy significantly reduces inter-subject variability. MMD-based methods like JAN and DJP-MMD improve transferability by aligning marginal distributions but lack explicit conditional distribution alignment, limiting their performance gains. Adversarial learning-based approaches such as DJDAN and GAT implicitly align domain features and improve class discriminability, but can be unstable and sensitive to hyperparameters. In our framework, the use of CS and CCS divergences offers a theoretically grounded and numerically stable alternative, enhancing alignment accuracy. The results highlight the advantage of selectively leveraging relevant source subjects and conducting both feature-level and decision-level alignment to mitigate inter-subject variability.

### B. Selective MSDA Under Large Source Base

To evaluate the practicality and scalability of the proposed source selection strategy in real-world scenarios with a large pool of source subjects, we conducted experiments on the full GigaDB dataset.

Each of the 10 subjects (s3, s5, s15, s18, s29, s31, s41, s43, s45, s46) from Dataset II was treated as a target domain, while the remaining 42 subjects served as potential sources. We applied a 25th percentile threshold on the source-target distances computed from BFM-extracted features to select approximately 12 relevant source subjects per target. Table III compares classification accuracies obtained using the proposed informed source selection against those from 12 randomly selected source subsets of similar size. The results show substantial variability in performance across random groups, with some groups (e.g., the first, fourth, and fifth) suffering from notably poor accuracies. In contrast, the proposed source selection method consistently achieves higher accuracies across most target subjects, demonstrating its effectiveness in identifying relevant sources and mitigating negative transfer.

Besides accuracy improvements, the source selection strategy significantly reduces computational overhead during training by excluding irrelevant or dissimilar sources. As illustrated in Fig. 2, when the filtering threshold is set at the 10th percentile, the average decoding accuracy reaches 77.21%. Increasing the threshold from the 10th to the 30th percentile dramatically increases the average training time per epoch from 3.14 seconds to 13.81 seconds, while yielding marginal or even slightly reduced performance. This highlights the efficiency benefits of tighter source selection, which is crucial for scaling MSDA to large datasets with numerous potential sources.

These findings emphasize the importance of source relevance and computational efficiency in MSDA for EEG decoding. By effectively filtering out distant or irrelevant subjects, the proposed framework not only enhances classification performance but also reduces training complexity, enabling faster model tuning and more practical deployment in real-world BCI applications.



TABLE I  
CROSS-SUBJECT ACCURACIES (MEAN  $\pm$  STD(%)) AND KAPPA ON DATASET I. BEST PERFORMANCES HIGHLIGHTED IN BOLD.

Methods	Subject									Avg. acc.	Kappa
	1	2	3	4	5	6	7	8	9		
EEGNet	72.92	64.58	79.17	78.47	86.11	74.31	83.33	79.86	82.64	77.93 $\pm$ 7.89	0.5586
ShallowConvNet	75.73	74.89	78.47	76.39	81.25	87.43	87.50	83.33	76.39	80.17 $\pm$ 5.83	0.6034
JAN	78.69	76.32	83.25	75.69	86.81	86.72	89.19	90.28	81.94	83.21 $\pm$ 6.17	0.6642
DJP-MMD	79.78	72.22	89.58	81.94	85.42	83.33	88.89	89.58	86.28	84.11 $\pm$ 6.32	0.6823
GAT	82.42	75.69	<b>93.06</b>	81.94	88.28	82.64	92.06	85.42	81.94	84.83 $\pm$ 6.13	0.6965
ASJDA	72.22	74.61	89.58	78.08	82.64	86.81	85.42	<b>90.97</b>	86.81	83.02 $\pm$ 7.54	0.6603
DJDAN	81.25	76.39	92.36	78.47	81.25	<b>88.19</b>	92.36	82.64	84.72	84.18 $\pm$ 6.42	0.6836
<b>Proposed</b>	<b>83.19</b>	<b>76.53</b>	91.74	<b>83.26</b>	<b>89.37</b>	81.46	<b>92.50</b>	90.14	<b>87.29</b>	<b>86.17 <math>\pm</math> 5.88</b>	<b>0.7233</b>

TABLE II  
CROSS-SUBJECT ACCURACIES (MEAN  $\pm$  STD(%)) AND KAPPA ON DATASET II. BEST PERFORMANCES HIGHLIGHTED IN BOLD.

Methods	Subject										Avg. acc.	Kappa
	1	2	3	4	5	6	7	8	9	10		
EEGNet	66.57	60.96	82.70	70.14	73.89	59.05	55.68	63.56	88.29	65.06	67.99 $\pm$ 12.92	0.3598
ShallowConvNet	73.92	67.63	75.05	71.55	75.23	63.65	70.56	67.70	78.02	66.37	70.97 $\pm$ 6.15	0.4194
JAN	78.27	71.38	80.72	73.75	79.46	76.84	73.05	70.30	87.35	70.28	76.14 $\pm$ 6.81	0.5228
DJP-MMD	76.31	<b>74.43</b>	78.26	71.85	73.62	77.94	70.22	71.43	82.45	71.52	74.80 $\pm$ 4.93	0.4961
GAT	74.25	70.36	83.73	69.32	77.45	78.73	<b>74.84</b>	72.84	90.45	73.64	76.56 $\pm$ 7.96	0.5312
ASJDA	79.03	69.72	78.16	69.52	67.46	72.56	64.68	<b>78.50</b>	89.15	72.42	74.12 $\pm$ 9.20	0.4824
DJDAN	78.36	70.87	80.53	72.73	74.67	<b>80.27</b>	74.38	74.54	90.12	70.94	76.74 $\pm$ 7.22	0.5348
<b>Proposed</b>	<b>80.52</b>	73.53	<b>85.15</b>	<b>74.48</b>	<b>81.42</b>	75.51	72.05	73.15	<b>92.75</b>	<b>75.52</b>	<b>78.41 <math>\pm</math> 7.95</b>	<b>0.5681</b>

TABLE III  
CROSS-SUBJECT PERFORMANCES OF DIFFERENT SOURCE GROUPS FROM THE GIGADB DATASET. BEST PERFORMANCES HIGHLIGHTED IN BOLD.

Methods	Subject										Avg. acc.	significance
	1	2	3	4	5	6	7	8	9	10		
Random Group 1	66.42	63.57	80.65	66.50	79.51	67.83	59.52	66.36	89.52	56.23	69.61 $\pm$ 14.13	$p < 0.01$
Random Group 2	73.85	<b>74.31</b>	79.27	73.03	72.65	70.95	71.18	<b>76.54</b>	85.42	74.85	75.21 $\pm$ 6.01	$p < 0.05$
Random Group 3	72.38	70.15	71.33	72.27	72.92	73.65	<b>78.63</b>	71.81	88.71	74.75	74.66 $\pm$ 6.29	$p < 0.01$
Random Group 4	71.38	72.81	79.52	65.15	69.81	71.57	63.82	70.55	89.17	65.67	71.95 $\pm$ 9.96	$p < 0.01$
Random Group 5	72.94	67.35	73.17	67.24	75.64	68.32	70.72	74.36	88.46	66.75	72.49 $\pm$ 8.47	$p < 0.01$
<b>Proposed</b>	<b>77.36</b>	70.87	<b>81.56</b>	<b>74.24</b>	<b>80.73</b>	<b>74.02</b>	74.31	72.35	<b>91.70</b>	<b>76.26</b>	<b>77.34 <math>\pm</math> 7.46</b>	—

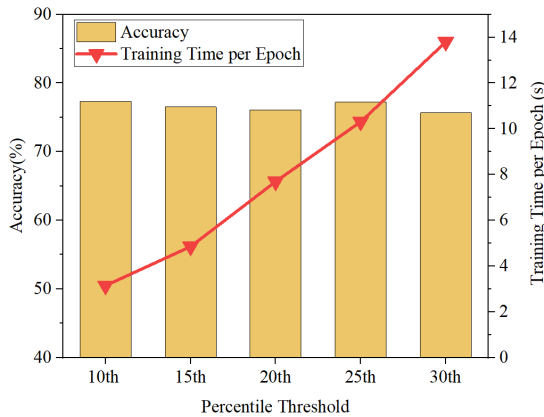


Fig. 2. Effect of selection threshold on training time and accuracy.

### C. Ablation Experiments

To evaluate the effectiveness of the key components in the proposed framework, we conducted ablation experiments on both datasets under consistent experimental settings. The

main contributions of our framework are the BFM-empowered source selection module and the MSDA leveraging CS divergences. Accordingly, we compared the following four variants:

- 1) Baseline EEGNet without DA or source selection
- 2) DA with FLA only
- 3) DA incorporating both FLA and DLA, but without source selection
- 4) Full BFM-MSDA framework, including source selection and MSDA

The cross-subject classification accuracies of each variant on both datasets are presented in Fig. 3. Incorporating FLA alignment alone improves the average accuracy by 5.17% and 4.11% over the baseline on Datasets I and II, respectively, demonstrating that aligning domain-level feature distributions significantly benefits MSDA. Adding conditional CS divergence for decision boundary alignment further enhances performance by approximately 1.91% on Dataset I and 3.14% on Dataset II. Finally, integrating the source selection module yields additional improvements of 1.15% and 2.37% on the respective datasets. Notably, the gains from decision boundary alignment and source selection are more pronounced



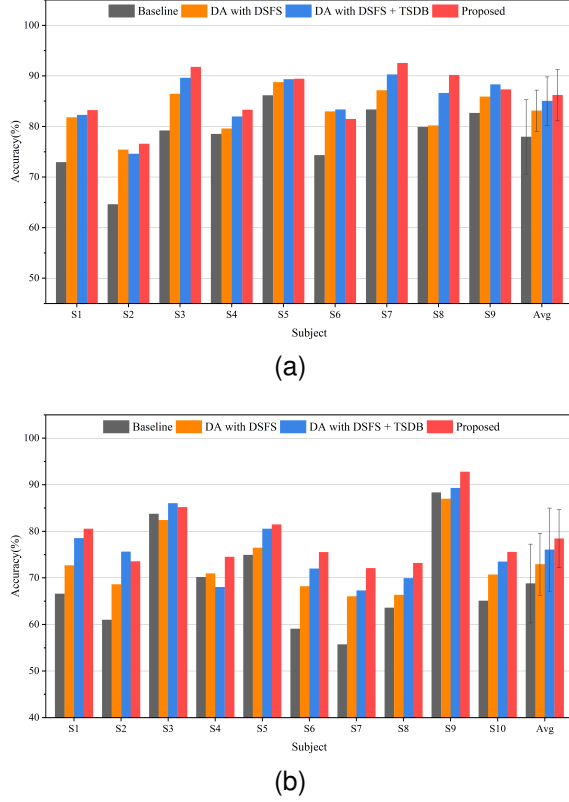


Fig. 3. Cross-subject classification accuracies of ablation variants on both datasets. (a) Dataset I. (b) Dataset II.

on Dataset II, which contains a larger and more diverse source pool. Overall, the cumulative improvements over the baseline reach 8.23% for Dataset I and 9.62% for Dataset II. Furthermore, these improvements are especially significant for subjects with lower baseline accuracies, highlighting the robustness of our approach in challenging cases.

#### D. Visualization

To comprehensively illustrate the effectiveness of the proposed BFM-MSDA framework, we performed several visualization analyses focusing on inter-subject relationships, feature discriminability in the target domain, and neurophysiological interpretability.

##### 1) Inter-subject Similarity via MDS and Heat Maps:

Multidimensional Scaling (MDS) [48] has been employed to visualize the proposed source selection process based on pairwise distances between subjects. MDS projects the high-dimensional distance matrix into a two-dimensional space, facilitating visual inspection of the relative similarities among subjects. Figs. 4a and 4b show the heat map and MDS visualization of inter-subject distances for Dataset I, respectively, while Figs. 4c and 4d present the corresponding heat map and MDS plot for Dataset II. The heat maps illustrate inter-subject distances computed by the pretrained LaBraM model using the CS divergence. The MDS plots reveal clusters of subjects with similar EEG feature distributions. The MDS visualization demonstrates that the selected source subjects lie closer to the corresponding target subject in the latent feature space.

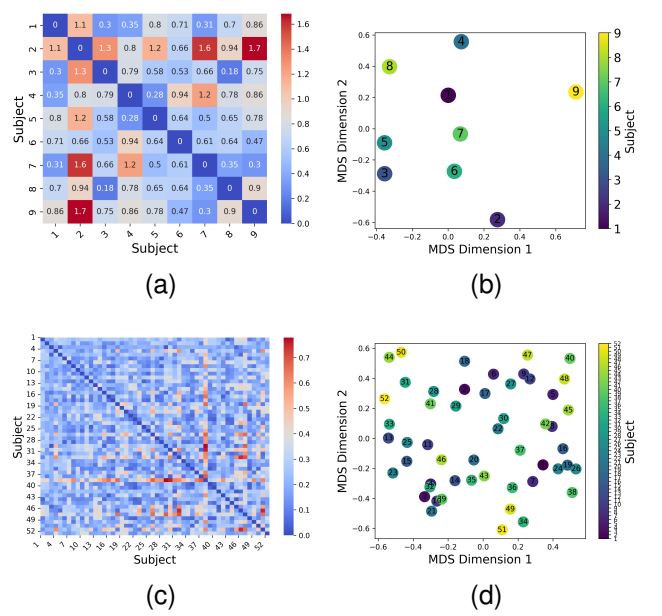


Fig. 4. Heat maps and MDS visualizations of pairwise distances for Datasets I and II. (a) Heat map of inter-subject distances for Dataset I. (b) MDS visualization of inter-subject distances for Dataset I. (c) Heat map of inter-subject distances for Dataset II. (d) MDS visualization of inter-subject distances for Dataset II.

##### 2) Feature Discriminability on Target Domain via t-SNE:

To further illustrate the adaptability and discriminative capability of the proposed BFM-MDA framework on the target domain, we visualized the latent features extracted by the feature extractor using t-distributed stochastic neighbor embedding (t-SNE), taking subject 1 from Datasets I and II as examples. Figs. 5 (a)–(e) present the t-SNE embeddings of target domain features for three cases on both datasets: the baseline EEGNet model without DA, the EEGNet enhanced with MSDA but without source selection, and the full BFM-MSDA framework.

From the visualizations, it is evident that the baseline model produces feature embeddings with significant overlap between different MI classes, indicating poor class separability and limited generalization to the target domain. Incorporating MSDA without source selection improves the clustering and separation of features, with more distinct groupings corresponding to different MI classes. The introduction of source selection further refines this separation, yielding clearly defined and well-separated clusters for each MI class. This improvement reflects the effectiveness of the BFM-guided source selection module in identifying relevant source subjects, which reduces negative transfer and enhances the alignment quality. The tighter and more compact clusters in (c) and (f) indicate that the learned feature representations are both more discriminative and better adapted to the target domain.

3) *Neurophysiological Interpretability via Topographic Maps:* To provide neuroscientific insight into the decoding performance, we visualized spatial patterns and model attention on EEG channels.

Fig. 6a shows the topographic maps of raw EEG data of subject s1 from Dataset I, highlighting sensor-level activity patterns during MI tasks. Fig. 6b displays Gradient-weighted

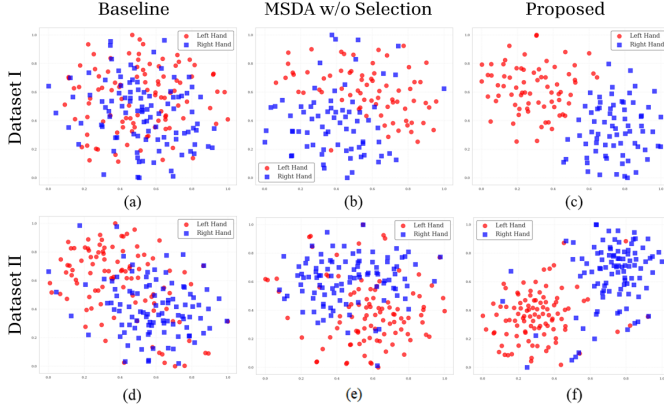


Fig. 5. t-SNE visualization of target domain features extracted by the feature extractor for subject 1 from Dataset I (top row) and Dataset II (bottom row). (a) and (d) baseline EEGNet without DA, (b) and (e) MSDA without source selection, and (c) and (f) full BFM-MSDA framework.

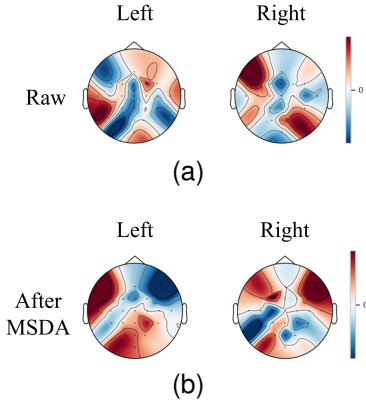


Fig. 6. EEG topography for subject 1 from Dataset I with different MI tasks. (a) Raw EEG signals averaged across all trials. (b) Grad-CAM of extracted features after BFM-MSDA.

Class Activation Mapping (Grad-CAM) [49] results for the feature extracted after the proposed BFM-MSDA method. Grad-CAM highlights the EEG channels and temporal regions most influential for model predictions.

Compared to the raw data, our method's Grad-CAM maps exhibit stronger and more focused activations over sensorimotor areas known to be involved in MI, such as the central and precentral regions. In addition, we observe spatial lateralization in S1 between brain hemispheres during left and right-hand MI, indicating significant ipsilateral activation and contralateral inhibition. This suggests that the proposed framework not only improves classification accuracy but also aligns closely with neurophysiological knowledge, reinforcing its interpretability and reliability for MI decoding.

#### E. Parameter Sensitivity Analysis

A comprehensive sensitivity analysis is conducted to evaluate the impact of the hyperparameters  $\alpha$  and  $\beta$ , which balance the FLA loss and the DLA loss, respectively, within the proposed framework. Specifically,  $\alpha$  was varied over the range  $[0, 0.9]$  and  $\beta$  over  $[0, 1.8]$ , while keeping all other parameters fixed.

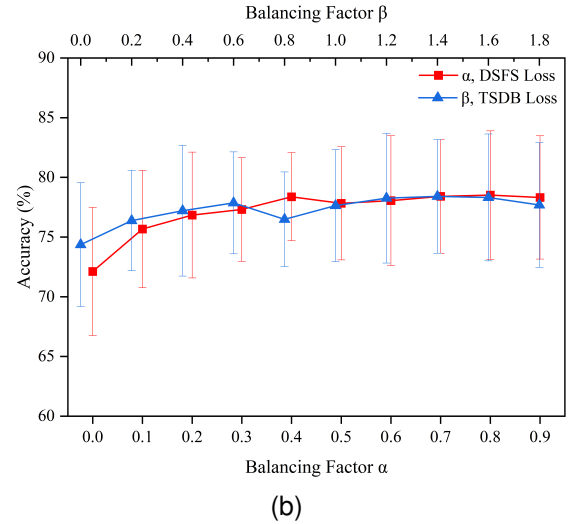
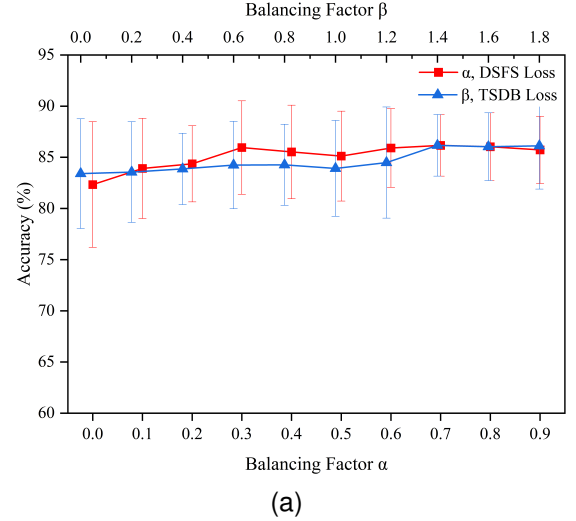


Fig. 7. Parameter sensitivity analysis of balancing factors for losses. (a) Influence of balancing factors for Dataset I. (b) Influence of balancing factors for Dataset II.

As shown in Fig. 7a and Fig. 7b, the framework exhibits stable and consistent performance across a wide range of  $\alpha$  and  $\beta$  values once the alignment losses are activated. For both datasets, the lowest classification accuracy occurs when  $\alpha = \beta = 0$ , corresponding to the absence of alignment regularization. Introducing the FLA and DLA alignment losses leads to noticeable improvements in accuracy. Notably, the performance gain attributed to the FLA alignment loss is more pronounced than that of the DLA loss. However, after the inclusion of these alignment terms, further tuning of  $\alpha$  and  $\beta$  results in only minor fluctuations in accuracy. This indicates that the proposed framework is robust to the specific choice of these hyperparameters.

#### VI. CONCLUSION

This study proposes a novel BFM-MSDA framework for cross-subject MI-EEG decoding that leverages the representational power of a pretrained large BFM for effective source selection, and multi-source alignment with CS and CCS divergences. The BFM-MSDA dynamically identifies relevant

source subjects through BFM-extracted features, which mitigates negative transfer and reduces computational complexity. By employing CS and CCS divergences, the framework explicitly performs feature-level and decision-level across multiple sources and the target, ensuring both domain invariance and discriminative power. Extensive experiments on two benchmark EEG datasets demonstrate that our method consistently outperforms SOTA baselines, achieving superior cross-subject generalization and robustness to inter-subject variability. The experiment on a large source pool further validates the scalability and practical implications of the proposed source selection strategy. To the best of our knowledge, the BFM-MSDA represents the first attempt to harness the power of BFMs within the DA framework for EEG-based MI decoding. Future research will explore an adaptive source selection method that dynamically determines the most relevant source domains without relying on a fixed percentile threshold. In addition, investigations will be conducted on more diverse datasets and tasks to further validate the robustness of the proposed framework.

#### APPENDIX

##### ESTIMATOR OF CAUCHY-SCHWARZ DIVERGENCE AND CONDITIONAL CAUCHY-SCHWARZ DIVERGENCE

In practice, the probability density function  $p(y|\mathbf{z})$  is unknown and must be estimated from finite samples. We adopt kernel-based empirical estimators for CS and CCS divergences, enabling efficient and nonparametric computation.

##### Empirical Estimator of CS Divergence [50]:

Given extracted features from two domains,  $\{\mathbf{z}_i^s\}_{i=1}^M$  from the source and  $\{\mathbf{z}_j^t\}_{j=1}^N$  from the target, the CS divergence between their distributions can be empirically estimated as:

$$\begin{aligned} \hat{D}_{\text{CS}}(p^s(\mathbf{z}); p^t(\mathbf{z})) &= \log \left( \frac{1}{M^2} \sum_{i=1}^M \sum_{j=1}^M \kappa(\mathbf{z}_i^s, \mathbf{z}_j^s) \right) \\ &+ \log \left( \frac{1}{N^2} \sum_{i=1}^N \sum_{j=1}^N \kappa(\mathbf{z}_i^t, \mathbf{z}_j^t) \right) \\ &- 2 \log \left( \frac{1}{MN} \sum_{i=1}^M \sum_{j=1}^N \kappa(\mathbf{z}_i^s, \mathbf{z}_j^t) \right), \end{aligned} \quad (15)$$

where  $\kappa(\cdot, \cdot)$  is a positive definite kernel function, typically the Gaussian kernel:

$$\kappa_\sigma(\mathbf{z}, \mathbf{z}') = \exp \left( -\frac{\|\mathbf{z} - \mathbf{z}'\|_2^2}{2\sigma^2} \right),$$

with bandwidth parameter  $\sigma$ .

In this work, the value of  $\sigma$  is adaptively set proportional to the median of pairwise distances between samples.

##### Empirical Estimator of CCS Divergence [45]:

Given features and predicted outputs from source and target domains,  $\{(\mathbf{z}_i^s, \hat{y}_i^s)\}_{i=1}^M$  and  $\{(\mathbf{z}_j^t, \hat{y}_j^t)\}_{j=1}^N$ , define Gram matrices for features and predictions as:

$$\begin{aligned} K_{ij}^s &= \kappa(\mathbf{z}_i^s, \mathbf{z}_j^s), & L_{ij}^s &= \ell(\hat{y}_i^s, \hat{y}_j^s), \\ K_{ij}^t &= \kappa(\mathbf{z}_i^t, \mathbf{z}_j^t), & L_{ij}^t &= \ell(\hat{y}_i^t, \hat{y}_j^t), \\ K_{ij}^{st} &= \kappa(\mathbf{z}_i^s, \mathbf{z}_j^t), & L_{ij}^{st} &= \ell(\hat{y}_i^s, \hat{y}_j^t), \\ K_{ij}^{ts} &= \kappa(\mathbf{z}_i^t, \mathbf{z}_j^s), & L_{ij}^{ts} &= \ell(\hat{y}_i^t, \hat{y}_j^s), \end{aligned}$$

where  $\kappa(\cdot, \cdot)$  and  $\ell(\cdot, \cdot)$  are kernel functions for features and predicted outputs, respectively.

The empirical CCS divergence estimator is approximated by:

$$\begin{aligned} \hat{D}_{\text{CCS}}(p^s(\hat{y}|\mathbf{z}); p^t(\hat{y}|\mathbf{z})) &\approx \log \left( \frac{\sum_{j=1}^M \sum_{i=1}^M K_{ji}^s L_{ji}^s}{\left( \sum_{i=1}^M K_{ji}^s \right)^2} \right) + \log \left( \frac{\sum_{j=1}^N \sum_{i=1}^N K_{ji}^t L_{ji}^t}{\left( \sum_{i=1}^N K_{ji}^t \right)^2} \right) \\ &- \log \left( \frac{\sum_{j=1}^M \sum_{i=1}^N K_{ji}^{st} L_{ji}^{st}}{\left( \sum_{i=1}^M K_{ji}^s \right) \left( \sum_{i=1}^N K_{ji}^{st} \right)} \right) \\ &- \log \left( \frac{\sum_{j=1}^N \sum_{i=1}^M K_{ji}^{ts} L_{ji}^{ts}}{\left( \sum_{i=1}^M K_{ji}^{ts} \right) \left( \sum_{i=1}^N K_{ji}^t \right)} \right). \end{aligned} \quad (16)$$

#### REFERENCES

- [1] B. J. Edelman, J. Meng, D. Suma, C. Zurn, E. Nagarajan, B. S. Baxter, C. C. Cline, and B. He, "Noninvasive neuroimaging enhances continuous neural tracking for robotic device control," *Science Robotics*, vol. 4, no. 31, p. eaaw6844, Jun. 2019.
- [2] F. Xu, J. Li, G. Dong, J. Li, X. Chen, J. Zhu, J. Hu, Y. Zhang, S. Yue, D. Wen, and J. Leng, "EEG decoding method based on multi-feature information fusion for spinal cord injury," *Neural Networks*, vol. 156, pp. 135–151, Dec. 2022.
- [3] H. Raza, A. Chowdhury, and S. Bhattacharyya, "Deep Learning based Prediction of EEG Motor Imagery of Stroke Patients' for Neuro-Rehabilitation Application," in *2020 International Joint Conference on Neural Networks (IJCNN)*. Glasgow, United Kingdom: IEEE, Jul. 2020, pp. 1–8.
- [4] H. Tayebi, S. Azadnajafabad, S. F. Maroufi, A. Pour-Rashidi, M. Khorasanizadeh, S. Faramarzi, and K. V. Slavin, "Applications of brain-computer interfaces in neurodegenerative diseases," *Neurosurgical Review*, vol. 46, no. 1, p. 131, May 2023.
- [5] C. Li, P. Li, Z. Chen, L. Yang, F. Li, F. Wan, Z. Cao, D. Yao, B.-L. Lu, and P. Xu, "Brain Network Manifold Learned by Cognition-Inspired Graph Embedding Model for Emotion Recognition," *IEEE Transactions on Systems, Man, and Cybernetics: Systems*, vol. 54, no. 12, pp. 7794–7808, Dec. 2024.
- [6] W. He, Y. Zhao, H. Tang, C. Sun, and W. Fu, "A Wireless BCI and BMI System for Wearable Robots," *IEEE Transactions on Systems, Man, and Cybernetics: Systems*, vol. 46, no. 7, pp. 936–946, Jul. 2016.
- [7] S. Aggarwal and N. Chugh, "Signal processing techniques for motor imagery brain computer interface: A review," *Array*, vol. 1–2, p. 100003, Jan. 2019.
- [8] B.-H. Lee, J.-H. Cho, and B.-H. Kwon, "Hybrid Paradigm-based Brain-Computer Interface for Robotic Arm Control," Dec. 2022.
- [9] A. Al-Saegh, S. A. Dawwd, and J. M. Abdul-Jabbar, "Deep learning for motor imagery EEG-based classification: A review," *Biomedical Signal Processing and Control*, vol. 63, p. 102172, Jan. 2021.
- [10] X. Chen, C. Li, A. Liu, M. J. McKeown, R. Qian, and Z. J. Wang, "Toward Open-World Electroencephalogram Decoding Via Deep Learning: A Comprehensive Survey," *IEEE Signal Processing Magazine*, vol. 39, no. 2, pp. 117–134, Mar. 2022.

- [11] P. Chen, Z. Gao, M. Yin, J. Wu, K. Ma, and C. Grebogi, "Multiattention Adaptation Network for Motor Imagery Recognition," *IEEE Transactions on Systems, Man, and Cybernetics: Systems*, vol. 52, no. 8, pp. 5127–5139, Aug. 2022.
- [12] W. Dang, D. Lv, M. Tang, X. Sun, Y. Liu, C. Grebogi, and Z. Gao, "Flashlight-Net: A Modular Convolutional Neural Network for Motor Imagery EEG Classification," *IEEE Transactions on Systems, Man, and Cybernetics: Systems*, vol. 54, no. 7, pp. 4507–4516, Jul. 2024.
- [13] S. Sakhavi, C. Guan, and S. Yan, "Learning Temporal Information for Brain-Computer Interface Using Convolutional Neural Networks," *IEEE Transactions on Neural Networks and Learning Systems*, vol. 29, no. 11, pp. 5619–5629, Nov. 2018.
- [14] H.-J. Ahn, D.-H. Lee, J.-H. Jeong, and S.-W. Lee, "Multiscale Convolutional Transformer for EEG Classification of Mental Imagery in Different Modalities," *IEEE Transactions on Neural Systems and Rehabilitation Engineering*, vol. 31, pp. 646–656, 2023.
- [15] D. Wu, X. Jiang, and R. Peng, "Transfer learning for motor imagery based brain-computer interfaces: A tutorial," *Neural Networks*, vol. 153, pp. 235–253, Sep. 2022.
- [16] D. Wu, Y. Xu, and B.-L. Lu, "Transfer Learning for EEG-Based Brain-Computer Interfaces: A Review of Progress Made Since 2016," *IEEE Transactions on Cognitive and Developmental Systems*, vol. 14, no. 1, pp. 4–19, Mar. 2022.
- [17] A. Gretton, K. M. Borgwardt, M. J. Rasch, and B. Sch, "A kernel two-sample test," *The Journal of Machine Learning Research*, vol. 13, no. 1, pp. 723–773, 2012.
- [18] M. Long, H. Zhu, J. Wang, and M. I. Jordan, "Deep Transfer Learning with Joint Adaptation Networks," in *Proceedings of the 34th International Conference on Machine Learning*. arXiv, Aug. 2017, pp. 2208–2217.
- [19] F. Wei, X. Xu, T. Jia, D. Zhang, and X. Wu, "A Multi-Source Transfer Joint Matching Method for Inter-Subject Motor Imagery Decoding," *IEEE Transactions on Neural Systems and Rehabilitation Engineering*, vol. 31, pp. 1258–1267, 2023.
- [20] W. Zhang and D. Wu, "Discriminative Joint Probability Maximum Mean Discrepancy (DJP-MMD) for Domain Adaptation," in *2020 International Joint Conference on Neural Networks (IJCNN)*. Glasgow, UK: IEEE, Apr. 2020, pp. 1–8.
- [21] X. Hong, Q. Zheng, L. Liu, P. Chen, K. Ma, Z. Gao, and Y. Zheng, "Dynamic Joint Domain Adaptation Network for Motor Imagery Classification," *IEEE Transactions on Neural Systems and Rehabilitation Engineering*, vol. 29, pp. 556–565, 2021.
- [22] F. Wei, X. Xu, X. Li, and X. Wu, "BDAN-SPD: A Brain Decoding Adversarial Network Guided by Spatiotemporal Pattern Differences for Cross-Subject MI-BCI," *IEEE Transactions on Industrial Informatics*, vol. 20, no. 12, pp. 14 321–14 329, Dec. 2024.
- [23] D. Liu, J. Zhang, H. Wu, S. Liu, and J. Long, "Multi-Source Transfer Learning for EEG Classification Based on Domain Adversarial Neural Network," *IEEE Transactions on Neural Systems and Rehabilitation Engineering*, vol. 31, pp. 218–228, 2023.
- [24] K. Liu, X. Luo, W. Zhu, Z. Yu, H. Yu, B. Xiao, and W. Wu, "Enhancing EEG-Based Cross-Subject Emotion Recognition via Adaptive Source Joint Domain Adaptation," *IEEE Transactions on Affective Computing*, pp. 1–13, 2021.
- [25] H. Altaheri, G. Muhammad, M. Alsulaiman, S. U. Amin, G. A. Altuwaijri, W. Abdul, M. A. Bencherif, and M. Faisal, "Deep learning techniques for classification of electroencephalogram (EEG) motor imagery (MI) signals: A review," *Neural Computing and Applications*, vol. 35, no. 20, pp. 14 681–14 722, Jul. 2023.
- [26] R. T. Schirmmeister, J. T. Springenberg, L. D. J. Fiederer, M. Glasstetter, K. Eggensperger, M. Tangemann, F. Hutter, W. Burgard, and T. Ball, "Deep learning with convolutional neural networks for EEG decoding and visualization," *Human Brain Mapping*, vol. 38, no. 11, pp. 5391–5420, Nov. 2017.
- [27] V. J. Lawhern, A. J. Solon, N. R. Waytowich, S. M. Gordon, C. P. Hung, and B. J. Lance, "EEGNet: A compact convolutional neural network for EEG-based brain-computer interfaces," *Journal of Neural Engineering*, vol. 15, no. 5, p. 056013, Oct. 2018.
- [28] D. Borra, S. Fantozzi, and E. Magosso, "Interpretable and lightweight convolutional neural network for EEG decoding: Application to movement execution and imagination," *Neural Networks*, vol. 129, pp. 55–74, Sep. 2020.
- [29] W. Tao, Z. Wang, C. M. Wong, Z. Jia, C. Li, X. Chen, C. L. P. Chen, and F. Wan, "ADFCNN: Attention-Based Dual-Scale Fusion Convolutional Neural Network for Motor Imagery Brain-Computer Interface," *IEEE Transactions on Neural Systems and Rehabilitation Engineering*, vol. 32, pp. 154–165, 2024.
- [30] H. He and D. Wu, "Transfer Learning for Brain-Computer Interfaces: A Euclidean Space Data Alignment Approach," *IEEE Transactions on Biomedical Engineering*, vol. 67, no. 2, pp. 399–410, Feb. 2020.
- [31] Y. Liang and Y. Ma, "Calibrating EEG features in motor imagery classification tasks with a small amount of current data using multisource fusion transfer learning," *Biomedical Signal Processing and Control*, vol. 62, p. 102101, Sep. 2020.
- [32] W. Zhang and D. Wu, "Manifold Embedded Knowledge Transfer for Brain-Computer Interfaces," *IEEE Transactions on Neural Systems and Rehabilitation Engineering*, vol. 28, no. 5, pp. 1117–1127, Apr. 2020.
- [33] S. Guo, Y. Wang, X. Zhang, and B. Tang, "A cross-session non-stationary attention-based motor imagery classification method with critic-free domain adaptation," *Biomedical Signal Processing and Control*, vol. 100, p. 107122, Feb. 2025.
- [34] H. Zhao, Q. Zheng, K. Ma, H. Li, and Y. Zheng, "Deep Representation-Based Domain Adaptation for Nonstationary EEG Classification," *IEEE Transactions on Neural Networks and Learning Systems*, vol. 32, no. 2, pp. 535–545, Feb. 2021.
- [35] Y. Song, Q. Zheng, Q. Wang, X. Gao, and P.-A. Heng, "Global Adaptive Transformer for Cross-Subject Enhanced EEG Classification," *IEEE Transactions on Neural Systems and Rehabilitation Engineering*, vol. 31, pp. 2767–2777, 2023.
- [36] J. Lee, J. W. Choi, and S. Jo, "Selective Multi-Source Domain Adaptation Network for Cross-Subject Motor Imagery Discrimination," *IEEE TRANSACTIONS ON COGNITIVE AND DEVELOPMENTAL SYSTEMS*, vol. 16, no. 3, 2024.
- [37] K. Yi, Y. Wang, K. Ren, and D. Li, "Learning topology-agnostic EEG representations with geometry-aware modeling," in *Advances in Neural Information Processing Systems*, A. Oh, T. Naumann, A. Globerson, K. Saenko, M. Hardt, and S. Levine, Eds., vol. 36. Curran Associates, Inc., 2023, pp. 53 875–53 891.
- [38] W.-B. Jiang, L.-M. Zhao, and B.-L. Lu, "Large Brain Model for Learning Generic Representations with Tremendous EEG Data in BCI," May 2024.
- [39] Z. Yuan, F. Shen, M. Li, Y. Yu, C. Tan, and Y. Yang, "BrainWave: A Brain Signal Foundation Model for Clinical Applications," Sep. 2024.
- [40] J. Wang, S. Zhao, Z. Luo, Y. Zhou, H. Jiang, S. Li, T. Li, and G. Pan, "CBraMod: A Criss-Cross Brain Foundation Model for EEG Decoding," Apr. 2025.
- [41] X. Zhou, C. Liu, Z. Chen, K. Wang, Y. Ding, Z. Jia, and Q. Wen, "Brain Foundation Models: A Survey on Advancements in Neural Signal Processing and Brain Discovery," Mar. 2025.
- [42] K. Kampa, E. Hasanbelliu, and J. C. Principe, "Closed-form cauchy-schwarz PDF divergence for mixture of Gaussians," in *The 2011 International Joint Conference on Neural Networks*. San Jose, CA, USA: IEEE, Jul. 2011, pp. 2578–2585.
- [43] A. T. Nguyen, Y. Gal, T. Tran, and A. G. Baydin, "Domain Invariant Representation Learning with Domain Density Transformations," in *35th Conference on Neural Information Processing Systems (NeurIPS 2021)*, 2021.
- [44] W. Yin, S. Yu, Y. Lin, J. Liu, J.-J. Sonke, and E. Gavves, "Domain Adaptation with Cauchy-Schwarz Divergence," May 2024.
- [45] S. Yu, H. Li, S. Løkse, R. Jenssen, and J. C. Principe, "The Conditional Cauchy-Schwarz Divergence with Applications to Time-Series Data and Sequential Decision Making," Apr. 2024.
- [46] C. Brunner, R. Leeb, G. R. Muller-Putz, and A. Schlogl, "BCI Competition 2008 – Graz data set A," *Institute for Knowledge Discovery (Laboratory of Brain-Computer Interfaces)*, Graz University of Technology, vol. 16, pp. 1–6, 2008.
- [47] H. Cho, M. Ahn, S. Ahn, M. Kwon, and S. C. Jun, "EEG datasets for motor imagery brain-computer interface," *GigaScience*, vol. 6, no. 7, p. gix034, Jul. 2017.
- [48] K. Q. Weinberger and L. K. Saul, "Unsupervised Learning of Image Manifolds by Semidefinite Programming," *International Journal of Computer Vision*, vol. 70, no. 1, pp. 77–90, Oct. 2006.
- [49] R. R. Selvaraju, M. Cogswell, A. Das, R. Vedantam, D. Parikh, and D. Batra, "Grad-CAM: Visual Explanations from Deep Networks via Gradient-Based Localization," in *2017 IEEE International Conference on Computer Vision (ICCV)*. Venice: IEEE, Oct. 2017, pp. 618–626.
- [50] R. Jenssen, J. C. Principe, D. Erdogmus, and T. Eltoft, "The Cauchy-Schwarz divergence and Parzen windowing: Connections to graph theory and Mercer kernels," *Journal of the Franklin Institute*, vol. 343, no. 6, pp. 614–629, Sep. 2006.